

Allocation Analysis of the Energy Storage System in Integrated Energy Systems Considering the Carbon Emissions and Cost

Wang Decheng^{1,2*}, Li Yan^{1,2}, Zhang Qun^{1,2}, Zhu Xiaojun^{1,2}, Wang Qiong^{1,2}

¹ State Grid Jiangsu Electric Power Design Consulting Co., Ltd Nanjing, China

² Jiangsu Branch of State Grid Economic and Technological Research Institute Co. Nanjing, China

Abstract. With the increasing integration of renewable energy into the power grid, the variability in its power generation has a growing impact on the stable energy supply of the system. The utilization of energy storage systems (ESSs) has been considered as an efficient approach to mitigate this effect. However, due to the different characteristics of different ESSs, it becomes an urgent issue about how to allocate the ESSs or combine different types of ESSs to maximize its performance. This study has constructed a new method to compare the performance of different ESSs, and analyze the strengths and weakness of mainstream ESSs with the real energy systems in Wuhan. It demonstrated that for short-term storage options such as superconducting energy storage, lithium-ion battery storage, and supercapacitor storage, larger capacities (2000kWh) yield better results. Conversely, the optimal allocation of long-term options like lead-acid batteries, flow batteries, and compressed air energy storage systems, depends on specific characteristics and wind patterns. Furthermore, this research also reveals that when considering the combination of involving both long-term (lead-acid battery) and short-term (superconducting battery) storages, it cannot simultaneously achieve optimal performance in terms of operating cost or carbon emissions reduction. For hybrid combinations such as supercapacitor-lithium-ion battery (short-term-short-term) or compressed air-energy-flow battery (long-term-long-term), it is crucial to ensure that the type with superior performance possesses maximum capacity.

1 Introduction

In recent years, in order to promote the implementation of the "dual-carbon" policy, various regions in China have increased the development of new energy sources^[1]. As industry is the largest contributor to carbon emissions in China efforts to reduce carbon emissions from energy consumption in industry have become a top priority^[2-4]. Therefore, many provinces and cities in China have begun to establish integrated energy systems equipped with high-capacity wind power and photovoltaic power generation equipment to meet their energy needs while reducing carbon emissions^[5]. However, due to the uncertainty of power generation from wind resources themselves, a high proportion of wind power generation will cause instability in the supply and demand of this integrated energy system^[6, 7]. The thermal power generation^[8-11], hydropower generation^[12, 13] and energy storage system^[8, 10, 14-19] are always employed to compensate the uncertainty in the energy supply-demand process^[20-22].

But thermal power generation and hydropower generation need to change their working conditions frequently to stabilize energy supply, which will cause the operational safety of the energy equipment itself as well as the operational economy to decline. Energy storage devices are widely used in regional

energy systems as a kind of energy equipment that can stabilize energy output and facilitate energy management and peak energy regulation. It can achieve the wind and solar power generation equipment to send out of the electric energy for storage, and according to the energy demand steadily into the energy supply network. This effectively solves the impact on other energy equipment and the power grid caused by the instability of power production due to the difference in the time distribution of wind and solar energy^[19].

Currently, energy storage systems are generally classified into two categories: physical storage and chemical storage^[23]. Physical storage includes pumped hydro storage, compressed air energy storage, flywheel energy storage, and superconducting energy storage, among others. Chemical storage encompasses lead-acid batteries, lithium-ion batteries, flow batteries, sodium-sulfur batteries, and supercapacitors. Different types of energy storage technologies possess their own technical advantages and limitations. Therefore, the capacity allocation and optimal selection of energy storage systems are crucial for the optimization of energy systems operation. Many scholars both domestically and internationally utilize heuristic algorithms^[24, 25], bio-inspired algorithms^[26, 27] or other novel algorithms^[28] to conduct research on optimal capacity allocation for energy storage. Some research findings indicate that technologies such

* Corresponding author: wangdc76@163.com

as compressed air energy storage, pumped hydro storage, flow batteries, and compressed air energy storage are more suitable for long-term storage with periods ranging from weeks to seasons^[29-31], while certain energy storage devices such as lithium-ion batteries and lead-acid batteries are more suitable for short-term (single-day/several days) peak shaving^[14, 16, 18]. However, there is still insufficient research on the adaptability of various types of energy storage systems to specific areas and the impact of different wind and solar power output characteristics on the optimal capacity allocation of different types of energy storage.

In summary, this study investigates the capacity adaptation of energy storage systems under changes in wind and solar power configurations in a park area, and further conducts performance comparisons among different types of energy storage. Based on this, the study comprehensively evaluates the economics of different energy storage devices by relying on two indicators: energy cost and carbon emissions of integrated energy systems. Finally, the study examines the charging and discharging characteristics of hybrid energy storage devices formed by combining two different types of energy storage equipment, as well as their applicability. The research findings can provide theoretical and data support for the development of relevant fields such as regional wind and solar power integration, energy storage facility construction, and energy system planning.

2 Model and methodology

This paper establishes a mathematical model for a comprehensive energy system at the park level, based on the actual situation of a certain park in Wuhan City. This model includes various energy devices such as photovoltaic power generation, wind power generation, and combined cooling, heating, and power (CCHP) systems. Performance analysis of the energy storage systems within the park is conducted using four indicators: total daily operating cost of the energy system, daily carbon emissions of the energy system, cost per unit of energy stored by the energy storage devices, and carbon emissions per unit of energy stored by the energy storage devices. The specific mathematical models for the devices and the definitions of evaluation indicators are as follows:

2.1 Mathematical model

2.1.1 Energy storage system

The energy storage system, serving as the primary focus of this study, is integrated within a comprehensive energy system to facilitate the absorption of unstable new energy generation and stabilize the output power of conventional power generation equipment^[32, 33]. Based on the different types of energy storage devices, a general mathematical model for energy storage units is constructed in this paper, as depicted^[34] in Equation (1) below:

$$SOC_{t+1} = (1 - \theta^{ESS}) \times SOC_t + \varepsilon_{ESS} \times \eta_{ec} \times P_{c,t}^{ESS} - \frac{P_{d,t}^{ESS}}{\eta_{ed}} \times (1 - \varepsilon_{ESS}) \quad (1)$$

$$s. t. \quad \begin{cases} 0 \leq SOC_t \leq SOC_{max} \\ 0 \leq P_{c,t}^{ESS} < P_{c,max}^{ESS} \\ 0 \leq P_{d,t}^{ESS} \leq P_{d,max}^{ESS} \end{cases}$$

wherein: SOC_t represents the state of charge of the energy storage system at time t , kWh; θ^{ESS} denotes the self-discharge rate of the energy storage system, expressed as a percentage, %; η_{ec} and η_{ed} represent the charging efficiency and discharging efficiency of the energy storage system, %. $P_{c,t}^{ESS}$ and $P_{d,t}^{ESS}$ denote the charging power supplied to the energy storage system by the system and the discharging power provided by the energy storage system to the system, respectively kW; SOC_{max} represents the maximum energy storage capacity of the system, kWh; $P_{c,max}^{ESS}$ and $P_{d,max}^{ESS}$ indicate the maximum charging and discharging power of the energy storage system, kW; ε_{ESS} is used to constrain the state of the energy storage system, where 1 represents the charging state and 0 represents the discharging state.

2.1.2 Combined cooling, heating and power (CCHP)

Combined cooling, heating, and power (CCHP) systems are among the primary equipment in advanced energy systems aimed at enhancing energy system efficiency. The gas turbine serves as the main component, utilizing the high-temperature exhaust gas discharged from micro gas turbine power generation to transfer the high-temperature heat into heat exchangers and bromine-lithium absorption refrigeration equipment through waste heat boilers. This process enables the secondary utilization of the high-temperature exhaust gas after combustion, effectively improving energy utilization efficiency and achieving multi-level utilization of energy^[35]. Currently, the energy utilization efficiency of CCHP systems using natural gas as fuel can reach up to 80%^[36]. In this paper, a conventional CCHP mathematical model based on heat-to-power ratio is employed to determine the power generation of the micro gas turbine based on CCHP cooling and heating power, subsequently calculating the volume of natural gas consumed by the CCHP system. The mathematical model^[37] is represented by Equation (2):

$$P_{ele,t}^{CCHP} = P_{gas,t}^{CCHP} \cdot \eta_{ele} = \left(\frac{P_{therm,t}^{CCHP}}{\eta_{therm}} + \frac{P_{cold,t}^{CCHP}}{\eta_{cold}} \right) \cdot \eta_{ele} \quad (2)$$

$$s. t. \quad \begin{cases} P_{energy,t}^{CCHP} \leq P_{energy,max}^{CCHP} \\ \eta_{energy} = f(P_{energy}^{CCHP}) \end{cases}$$

$energy \in \{ele, therm, cold, gas\}$

wherein: $P_{energy,t}^{CCHP}$ represents the power generation capacity of the CCHP system at time t , kW; $P_{gas,t}^{CCHP}$ denotes the thermal power of natural gas combustion in the CCHP system at time t , kJ/s; η_{energy} represents the ratio of the corresponding energy power to the thermal power of natural gas combustion, %; f represents a polynomial relationship of the CCHP's various energy efficiencies with the energy power of the CCHP system at that time. The model in this paper includes a CCHP device with a total power of 2000 kW.

2.1.3 Gas boiler

The gas boiler primarily serves to supplement the thermal load within the supply energy area of the entire comprehensive energy system. The specific mathematical model[38] is represented by Equation (3):

$$P_{therm,t}^{GB} = \eta^{GB} P_{gas,t}^{GB} \quad (3)$$

$$s. t. \begin{cases} \eta_{GB} = f(P_{therm,t}^{GB}) \\ 0 \leq P_{h,t}^{GB} \leq P_{h,max}^{GB} \end{cases}$$

where, $P_{therm,t}^{GB}$ represents the heat supply power of the gas boiler at time t , in kW; η^{GB} represents the thermal efficiency of the gas boiler; gas, $P_{gas,t}^{GB}$ represents the heat value of natural gas supplied to the gas boiler at time t , in kJ/s; $P_{therm,max}^{GB}$ represents the maximum heat supply power of the gas boiler, in kW. This model includes a gas boiler with a rated power of 500 kW and an efficiency of 95%.

2.1.4 Utility grid

The grid plays a crucial role as a supplementary component of the integrated energy system, maintaining the balance between supply and demand. When the system generates more electricity than demanded, the surplus energy is sold to the grid, whereas when the system generates less electricity than required, it purchases electricity from the grid. In this study, the purchasing price from the grid is referenced from the electricity grid prices in Hubei Province, as depicted in Equation (4)

$$EP_b = \begin{cases} 0.2817 \text{ CNY/kWh, } 23:00 \sim 8:00 \\ 0.5869 \text{ CNY/kWh, } 8:00 \sim 10:00 \text{ } 16:00 \sim 20:00 \text{ } 22:00 \sim 23:00 \\ 0.8745 \text{ CNY/kWh, } 10:00 \sim 16:00 \\ 1.0564 \text{ CNY/kWh, } 20:00 \sim 22:00 \end{cases} \quad (4)$$

2.1.5 Heat pump

The heat pump, as an efficient energy conversion device, is widely utilized in integrated energy systems to meet the

$$s. t. \begin{cases} P_{ele,t}^{IES} + P_{c,t}^{ESS} \cdot (1 - \varepsilon_{ESS}) + P_{ele,t}^{HP} = P_{d,t}^{CCHP} + P_{d,t}^{ESS} \cdot \varepsilon_{ESS} + P_{GF,t} + P_{FD,t} + P_t^{grid} \\ P_{therm,t}^{IES} = P_{therm,t}^{CCHP} + P^{HP} \times \varepsilon_{HP} + P_{therm,t}^{GB} \\ P_{cold,t}^{IES} = P_{cold,t}^{CCHP} + P^{HP} \times (1 - \varepsilon_{HP}) + P_{cold,t}^{GB} \end{cases} \quad (8)$$

3 Objective and evaluation metrics

3.1 Total energy cost and carbon emissions

The overall energy system cost, as a crucial metric for evaluating energy storage systems, primarily encompasses the electricity and natural gas consumption costs of the system. The specific calculation is outlined as follows in Equation (9):

$$\text{Total Cost} = \sum_{t=1}^T \left[\left(\frac{P_{ele,t}^{CCHP}}{\eta_{ele}} + \frac{P_{therm,t}^{GB}}{\eta_{GB}} \right) \times \frac{1}{\mu} \times p_{gas} + P_t^{grid} \times p_t^{grid} \right] \quad (9)$$

where, Total Cost represents the total cost required for the operation of the integrated energy system, in CNY; μ represents the heat value of natural gas, in kJ/Nm³; p_{gas} represents the purchase cost of gas for the energy system, at

demand for heating and cooling in various sectors. It utilizes electricity to transfer heat energy from a low-temperature heat source to a high-temperature heat sink. Particularly in industries with high demand for low-temperature heat, such as livestock farming and agriculture, heat pumps have significant potential for carbon emissions reduction.

The model of the heat pump system used in this study is represented by Equation (6)^[39]

$$P^{HP} = \varepsilon_{HP} \cdot COP_t^{HP} \cdot P_{ele}^{HP} + (1 - \varepsilon_{HP}) \cdot COP_c^{HP} \cdot P_{ele}^{HP} \quad (5)$$

$$s. t. \quad 0 \leq P^{HP} \leq (1 - \varepsilon) \cdot P^{HP} + \varepsilon \cdot P^{HP}$$

where, P^{HP} represents the heating/cooling power of the heat pump at the given time, in kW; ε_{HP} represents the state of the heat pump, where 1 indicates heating mode and 0 indicates cooling mode. COP stands for the coefficient of performance of the heat pump, representing its efficiency in heating or cooling. P_{ele}^{HP} represents the electrical power consumption of the heat pump, in kW.

The model considered in this paper involves two heat pump units, each with a power of 2800 kW and a coefficient of performance (COP) of 2.1 for heating and 1.8 for cooling.

2.2 Constraints

The overall energy demand of the park includes three types: electricity, heat, and cooling. Based on the principle of energy conservation, this paper proposes the overall energy constraint equation for the park, as shown in Equation (8):

where, $P_{energy,t}^{IES}$ represents the energy demand of the park at time t , $energy \in \{ele, therm, cold, gas\}$, kW; P_t^{grid} represents the electrical energy exchanged between the integrated energy system and the grid at time t , with buying electricity denoted as "+" and selling electricity denoted as "-", measured in kW.

3.094 CNY/Nm³; p_t^{grid} represents the selling price of electricity from the grid at time t , in CNY/kWh.

Additionally, carbon emissions, as a critical assessment factor in the current energy system, are also considered in this research. The total carbon emissions of the integrated energy system mainly consist of carbon emissions from burning natural gas and carbon dioxide emissions generated by purchasing electricity from the grid, calculated as shown in equation (10).

$$\text{Car.Emi.} = \sum_{t=1}^T \left[\left(\frac{P_{ele,t}^{CCHP}}{\eta_{ele}} + \frac{P_{therm,t}^{GB}}{\eta_{GB}} \right) \times \frac{1}{\mu} \times \zeta_{gas} + P_t^{grid} \times \zeta_{grid} \right] \quad (10)$$

where, $Car.Emi.$ represents the total carbon emissions during the operation, kg; ζ_{gas} represents carbons emission per unit volume of natural gas burned, kg/Nm³; ζ_{grid} represents emission per unit kWh of electricity produced by the grid, kg/kWh.

3.2 Energy cost and carbon emission intensity

Furthermore, this study also considers the unit energy cost and carbon emission intensity of the comprehensive energy system under different energy storage technology usage. The specific computational formula is given by Equation (11):

$$CPE = \frac{Total\ Cost}{\sum_{t=1}^T P_{ele}^{HP} + P_{ele,t}^{IES}} \quad (11)$$

where, CPE represents the cost required for the comprehensive energy system to output 1 kWh of electricity, CNY/kWh.

The carbon emission intensity is the amount of carbon dioxide emitted per kWh of electricity produced and used by the comprehensive energy system, calculated by the formula as follows:

$$CEPE = \frac{Car.EMI.}{\sum_{t=1}^T P_{ele}^{HP} + P_{ele,t}^{IES}} \quad (12)$$

CEPE represents the amount of carbon dioxide emitted per kWh of electricity output by the comprehensive energy system, kg/kWh.

3.3 Multi-objectives particle swarming algorithm

Through the construction of a comprehensive energy system model and objective functions, this study proposes to use a multi-objective particle swarm optimization algorithm to compare and analyze the impact of different energy storage systems on the economic viability and carbon emissions of the energy system. Particle swarm optimization (PSO) is a bio-inspired heuristic algorithm based on the collective behavior of birds, and it is widely used as a population-based optimization algorithm, particularly in energy system scheduling and optimization^[11, 17]. The specific computational process is illustrated in Figure 1.

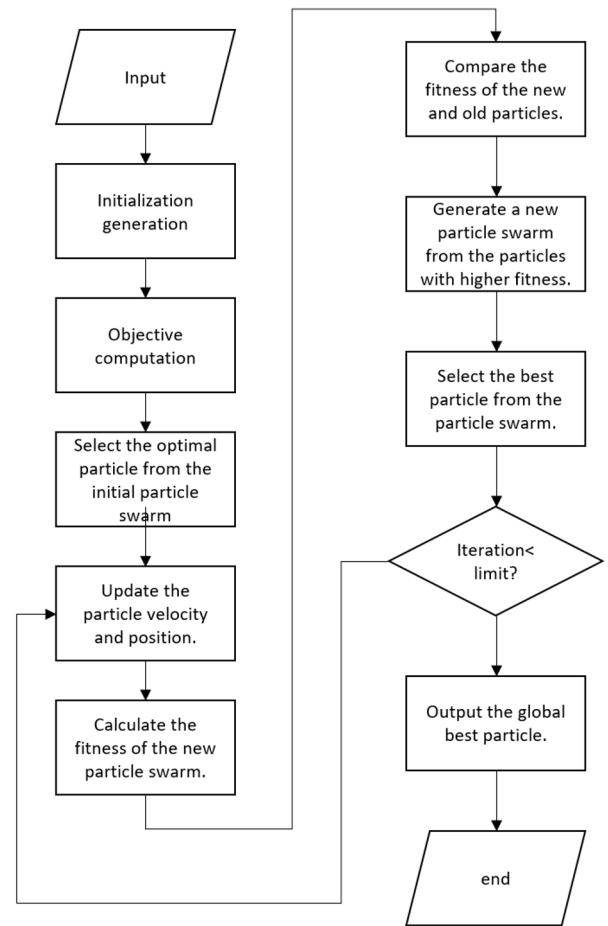


Fig. 1. Flowchart of particle swarm optimization algorithm

- Step 1: Initialize the system by generating N particles, where each particle's position represents the power generation (or consumption) / heat output of each energy device in the distributed energy system at each time step.
- Step 2: Based on the operational status of each device within the particles, calculate the energy system's operating cost, carbon emissions, energy output, and the absolute difference between energy production and load demand. Develop an objective function to quantify the fitness of each particle.
- Step 3: Compare the fitness of different particles and select the particle with the highest fitness. Adjust the positions of other particles and recalculate their fitness accordingly.
- Step 4: Iterate through the process until the particle with the optimal fitness is found, representing the energy output of all devices under the most optimal conditions.

4 Results

4.1 Cost analysis

This study initially examines the optimal capacity configuration issue for the currently matured lithium iron

phosphate batteries as energy storage devices in the energy system. The results, as depicted in Figure 2, indicate that as the capacity of lithium iron phosphate batteries increases from 0 kWh to 10,000 kWh, the unit energy cost of the entire integrated energy system first rises and then declines:

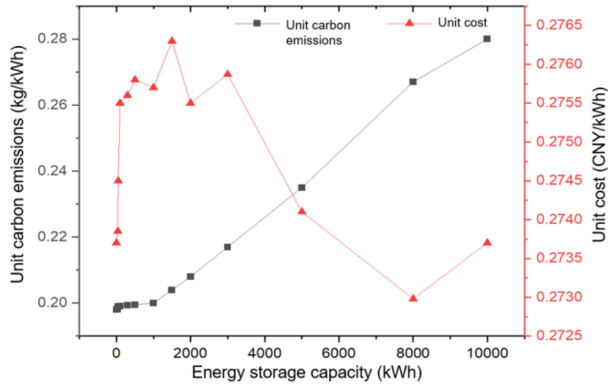
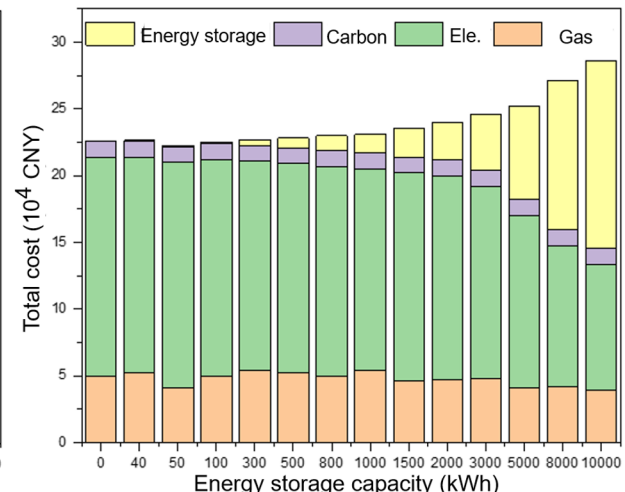
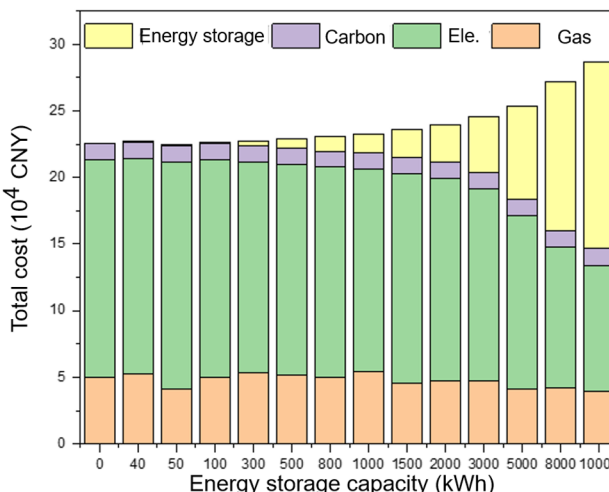
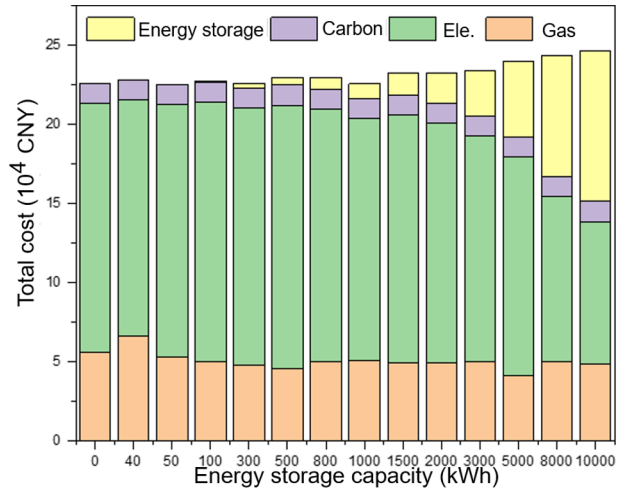
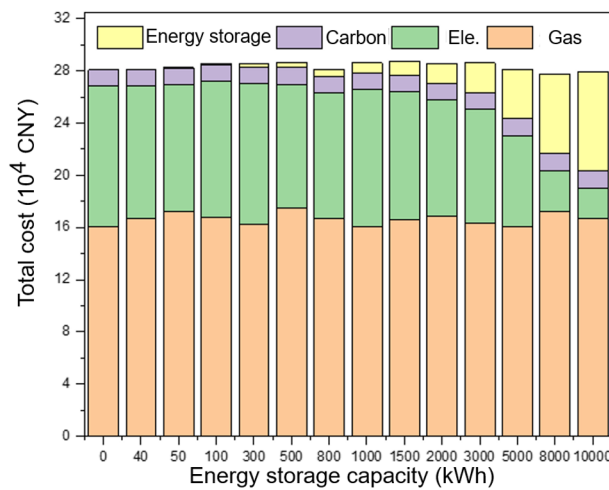


Fig. 2. Changes in carbon emissions and costs per unit of different energy storage capacities

1. Within the range of 0 to 1500 kWh, the low capacity of lithium iron phosphate batteries leads to insufficient benefits to offset the investment costs incurred during construction, resulting in an increase in the unit energy output cost of the energy system.

2. Within the range of 1500 to 8000 kWh, as the capacity of lithium iron phosphate batteries increases, the benefits obtained by the energy system from the price difference between peak and off-peak electricity prices exceed the increase in investment costs or the increase in energy costs due to self-consumption of energy. The inflection point occurs at around 3000 kWh.



(a)Lithium-ion Battery (LiFePO₄) (b)Trivalent Lithium-ion Battery (c)Sodium-Sulfur Battery (d)All-Vanadium Flow Battery

Fig. 3. Energy costs for different storage capacities

3. Within the range of 8000 to 10,000 kWh, as the capacity of lithium iron phosphate batteries increases, the investment costs on the batteries rise continuously. However, the additional

daily output of the integrated energy system cannot meet the storage needs of the energy storage due to the surplus capacity

of the energy storage, resulting in an increase in the unit output energy cost of the integrated energy system.

Further comparison of the performance of different types of energy storage batteries, including ternary lithium-ion batteries, sodium-sulfur batteries, and an all-vanadium redox flow battery, in the energy system reveals significant differences in their performance, as illustrated in Figure 3:

1. As the capacity of lithium iron phosphate batteries increases, the overall carbon emissions per unit of energy gradually rise (Figure 3a). The main reasons for this are twofold: firstly, energy storage devices consume additional electricity during their charge and discharge cycles, and self-discharge of energy stored in the energy storage device leads to energy consumption, resulting in an increase in carbon emissions per unit of energy load; secondly, carbon emissions occur during the construction of the energy storage system, and the amount of emissions increases with the system's capacity. To reduce the increase in carbon emissions caused by this, it is feasible to increase the number of charge and discharge cycles and the amount of charge and discharge energy throughout the lifecycle of the energy storage system.

2. As shown in Figure 3(b), the economic viability of ternary lithium-ion battery energy storage varies significantly with capacity. For lithium-ion battery energy storage, the benefits obtained from carbon emissions increase relatively slowly with increasing storage capacity. From 500 kW onwards, the benefits from capacity tariffs increase rapidly, with capacity tariffs contributing to about one-third of the total benefits at a capacity of 10,000 kW. However, the benefits from electricity charges and gas charges decrease continuously.

3. For sodium-sulfur batteries (Figure 3c), the total cost variation follows a similar trend to lithium-ion batteries, but sodium-sulfur batteries are more sensitive to capacity costs. When the installed capacity of sodium-sulfur batteries reaches 10,000 kW, capacity costs account for nearly half of the total costs, exceeding those of lithium-ion battery energy storage.

4. Regarding all-vanadium redox flow battery energy storage (Figure 3d), its economic viability changes in a manner similar to sodium-sulfur batteries. From the perspective of total contract and cost structure, further improvement in economic viability is needed compared to lithium-ion battery energy storage.

4.2 Analysis of Cost for Energy Storage Systems of Different Types with the Same Capacity

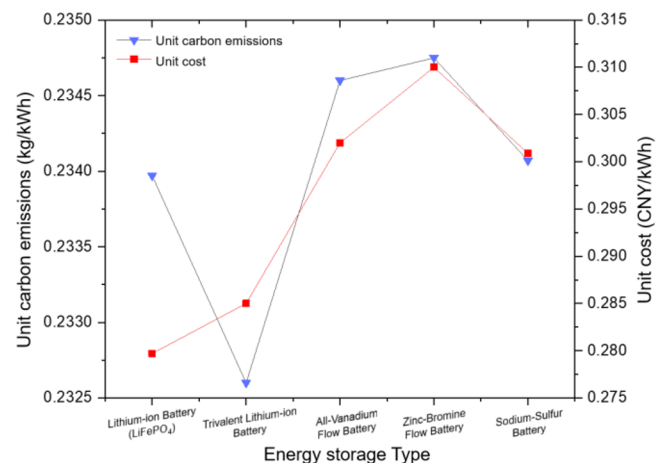
Building upon the economic and carbon emission analysis of single energy storage systems within the integrated energy system, this study undertakes a comparative analysis of the economic viability and suitability of multiple types of energy storage devices. The chosen energy storage system characteristics are outlined in Table 1 to facilitate this comparative analysis.

Table.1 Cost of electricity and conversion efficiency of different energy storage types

Energy Storage Type	Energy Storage Cost [CNY/(kW·h)]	Efficiency/%
---------------------	----------------------------------	--------------

Lithium-ion Battery (LiFePO ₄)	0.5~0.9	90~95
Trivalent Lithium-ion Battery	0.6~1.0	90~95
All-Vanadium Flow Battery	0.7~1.0	65~80
Zinc-Bromine Flow Battery	0.8~1.2	65~80
Sodium-Sulfur Battery	0.9~1.2	>90

The comparative analysis results, as illustrated in Figure 4, reveal that among the five different types of energy storage devices, the two types of flow batteries and sodium-sulfur batteries exhibit higher levels of both cost per kilowatt-hour (kWh) and carbon emissions per kWh compared to the two lithium-ion batteries (lithium iron phosphate and trivalent lithium-ion). Specifically, the zinc-bromine flow battery demonstrates the highest carbon emissions per kWh (0.2348 kg/kWh) and the highest cost per kWh (0.3095 CNY/kWh). On the other hand, the lithium iron phosphate battery exhibits the lowest cost per kWh, at 0.2793 CNY/kWh, while the trivalent lithium-ion battery shows the lowest carbon emissions per kWh, at 0.2326 kg/kWh.



In the context of these five energy storage device scenarios, the integrated energy system utilizing lithium-ion batteries generally presents lower overall unit energy costs and carbon emissions per unit energy. Conversely, systems employing flow batteries tend to exhibit higher unit energy costs and carbon emissions per unit energy. This discrepancy is primarily attributed to two factors: firstly, the overall cost per kWh of flow batteries is higher, leading to an increase in unit energy load; secondly, flow batteries have lower charge-discharge efficiency, resulting in higher energy consumption during the storage and discharge processes and consequently higher carbon emissions.

4.3 Analysis of Best Capacity Configuration for Different Energy Storage

The continuous advancement of wind-solar power generation has increased the demand for energy storage construction. Therefore, this section investigates the impact of

changes in wind-solar power capacity configuration and generation characteristics on energy storage system capacity configuration. Subsequently, it conducts an analysis of the optimal capacity configuration for various types of energy storage under wind-solar power generation characteristics.

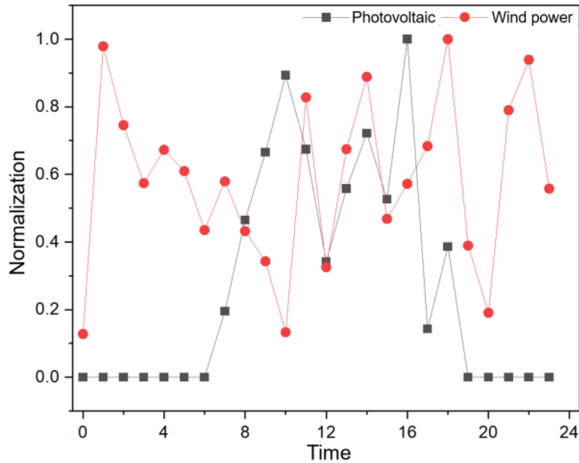
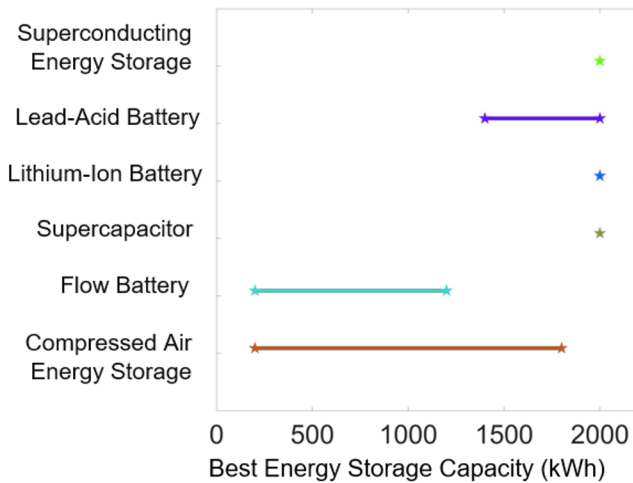


Fig. 4. Power distribution characteristic of typical solar and wind energy in Wuhan

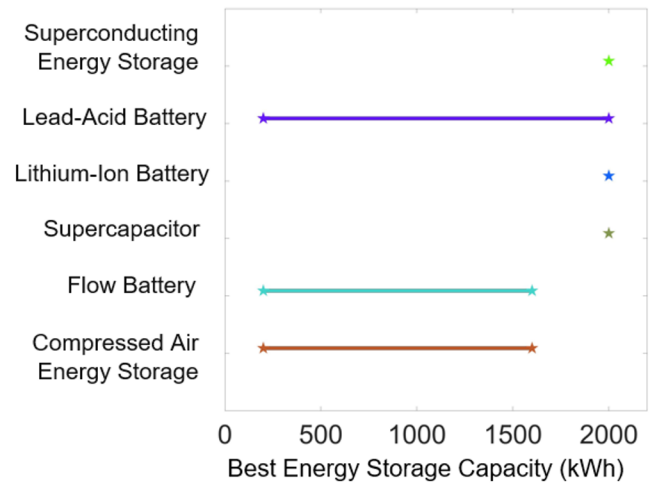
Based on the typical wind-solar power characteristic curve in Wuhan city (Figure 5), this study establishes twenty scenarios where the total daily wind and solar power generation ranges from 10% to 100% of the daily energy demand of the park. These scenarios are utilized to investigate the optimal configuration of different types of energy storage under varying generation conditions.

Table. 2 Scenario Setting for Proportions of Photovoltaic and Wind Power Generation

Photovoltaic		Wind power	
Scenario	Proportion	Scenario	Proportion
1	10%	11	10%
2	20%	12	20%
⋮	⋮	⋮	⋮
10	100%	20	100%



(a) without photovoltaic power



(b) without wind power

Fig. 5. Optimal capacity of different hybrid energy storage with different renewable energy generation characteristics

Based on the aforementioned twenty scenarios, simulations were conducted to analyze and determine the optimal storage capacity configuration ranges for the five types of energy storage. Long-term and short-term energy storage exhibit distinct distribution characteristics. Short-term storage devices such as superconducting energy storage, lithium-ion battery storage, and supercapacitor storage demonstrate optimal ranges at maximum capacity values (2000 kWh) for different capacity configurations of renewable energy sources, primarily due to their rapid peak shaving and frequency regulation capabilities. Conversely, long-term storage devices such as lead-acid batteries, flow batteries, and compressed air energy storage present optimal ranges for different capacity configurations of renewable energy sources, with some disparity in optimal ranges for different characteristics. Under the wind power

characteristics in Wuhan, the optimal range for lead-acid batteries is [1400 kWh, 2000 kWh], for flow batteries it is [100 kWh, 1200 kWh], and for compressed air energy storage it is [100 kWh, 1800 kWh]. Conversely, under the characteristics of solar power generation in Wuhan, the optimal range for lead-acid batteries is [100 kWh, 2000 kWh], for flow batteries it is [100 kWh, 1600 kWh], and for compressed air energy storage it is [100 kWh, 1600 kWh].

In summary, under equivalent wind and solar load conditions, the operational costs of integrated energy systems vary, with discrepancies increasing as the proportion of solar and wind power increases. When generating the same amount of electricity, the operational costs of photovoltaic (PV) systems are lower than those of wind power systems. This difference stems from the superior spatiotemporal

characteristics of PV generation, which exhibit a higher degree of alignment with user demand patterns, thus reducing the need for energy transfer over space and time and subsequently lowering operational costs. In this section, simulations were conducted for five additional energy storage types, delineating their optimal storage capacity ranges. Short-term energy storage devices such as superconducting energy storage, lithium-ion battery storage, and supercapacitor storage exhibit optimal ranges at maximum capacity values, primarily due to their rapid peak shaving and frequency regulation capabilities. Conversely, long-term energy storage devices such as lead-acid batteries, flow batteries, and compressed air energy storage present optimal ranges for different capacity configurations of renewable energy sources, varying due to their distinct characteristics. Under the wind and solar conditions in Wuhan, optimal ranges for various long-term energy storage types exhibit some disparity. Given the inherent differences among energy storage technologies, this paper further investigates the optimal configuration of hybrid energy storage systems within the energy system.

5 CASE STUDY

Due to the significant differences in the short-term and long-term energy storage capabilities of different types of energy storage systems, mixed energy storage has become one of the solutions to address the incomplete capabilities of single energy storage systems^[17]. Therefore, building upon the optimization of single energy storage capacity configuration, this paper further proposes an analysis method for the optimal ratio of mixed energy storage device capacities, analyzing the best capacity ratio for two different types of energy storage systems in the energy system. The specific steps are as follows, as shown in Figure 7:

Clarify the policy parameters, equipment parameters, and regional load-related information of the energy system environment. Regarding policy parameters, it is necessary to specify the energy prices in various markets such as electricity trading, carbon trading, and natural gas trading in the energy market. Regarding equipment parameters, it is essential to specify various parameters of renewable energy equipment within the energy system (such as wind turbine capacity,

Establish an operation optimization scheduling model for the mixed energy storage system. By referring to existing energy systems or future planned energy systems, establish a matching mathematical model for the energy system. Utilize appropriate intelligent optimization algorithms, input the required parameters, and set the benefit functions related to factors such as energy system operation and maintenance costs, construction costs, carbon emissions, and energy supply-demand balance stability to optimize the internal devices of the energy system within the feasible domain. Eventually, obtain the optimal benefits of the energy system over a certain period.

By comparing the optimal benefits of the energy system under different mixed energy storage capacity configurations, analyze and determine the optimal mixed energy storage capacity and its internal capacity configuration.

Based on the above ideas, this section divides the energy storage system into three groups according to the energy storage characteristics and using the current conventional mixed energy storage grouping method (Table 3). For each of the three different combinations, while ensuring the total capacity of mixed energy storage remains consistent, the study varies the capacity ratios between different types of energy storage devices within the mixed energy storage, aiming to investigate the characteristics between different types of energy storage combinations and the capacity configuration characteristics of different types of energy storage within the same combination.

The state of charge (SOC) distribution of two types of energy storage devices within the mixed energy storage under a capacity ratio of 7:3 is illustrated in Figure 8. For example, in the case of supercapacitors 700 kW and lithium-ion batteries 300 kW, and lead-acid batteries 700 kW and superconducting energy storage 300 kW, most energy storage devices are in a charging state during the first half of the day (00:00 to 12:00), while most are in a discharging state during the second half of

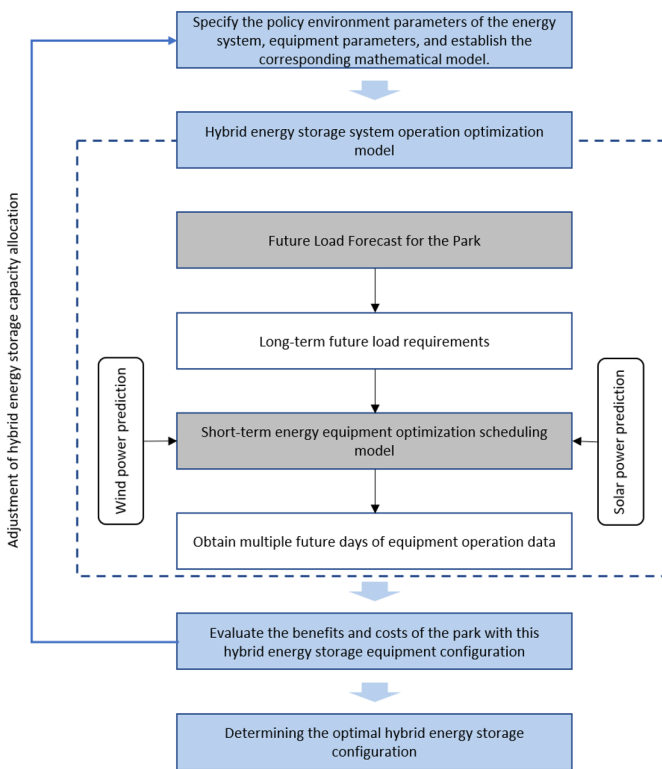


Fig. 6. Flowchart of optimal ratio analysis method for hybrid energy storage equipment

photovoltaic unit capacity, etc.), various internal characteristic parameters of required energy storage devices, and other parameters of energy production and conversion devices. For regional load, historical load data can be used for already commissioned energy systems; for early-stage energy equipment capacity optimization, reasonable assessments of energy loads can be made based on industry peers' energy loads and requirements for energy equipment.

the day (12:00 to 24:00). Long-term energy storage devices such as lead-acid batteries can continuously generate full-load

Table. 3 Characteristic parameters of hybrids energy storage systems

	Group 1 (Long-Long)		Group 2 (Short-Short)		Group 3 (Long-short)	
	Compressed air energy storage	Flow Battery	Supercapacitor	Lithium-Ion Battery	Lead-Acid Battery	Superconducting Energy Storage
Discharge rate	0.5	1	0.95	0.85	0.7	0.95
Efficiency	0.45	0.7	0.9	0.95	0.9	0.8
Volumetric Power Density	0.4	1	20000	5000	0.0002	2600
Volumetric Energy Density	4	20	20	300	0.001	6
Discharging Hours	5	20	1	1	3.5	1
Self-Discharge Rate	0.1	0	0.3	0.01	0.01	0.12
Cost per kWh	0.21	0.52	0.73	0.48	0.4	0.7
Carbon Emissions per kWh	30	28	38	78	30	20



Fig. 7. Charge and discharge power of hybrid energy storage battery at each time node

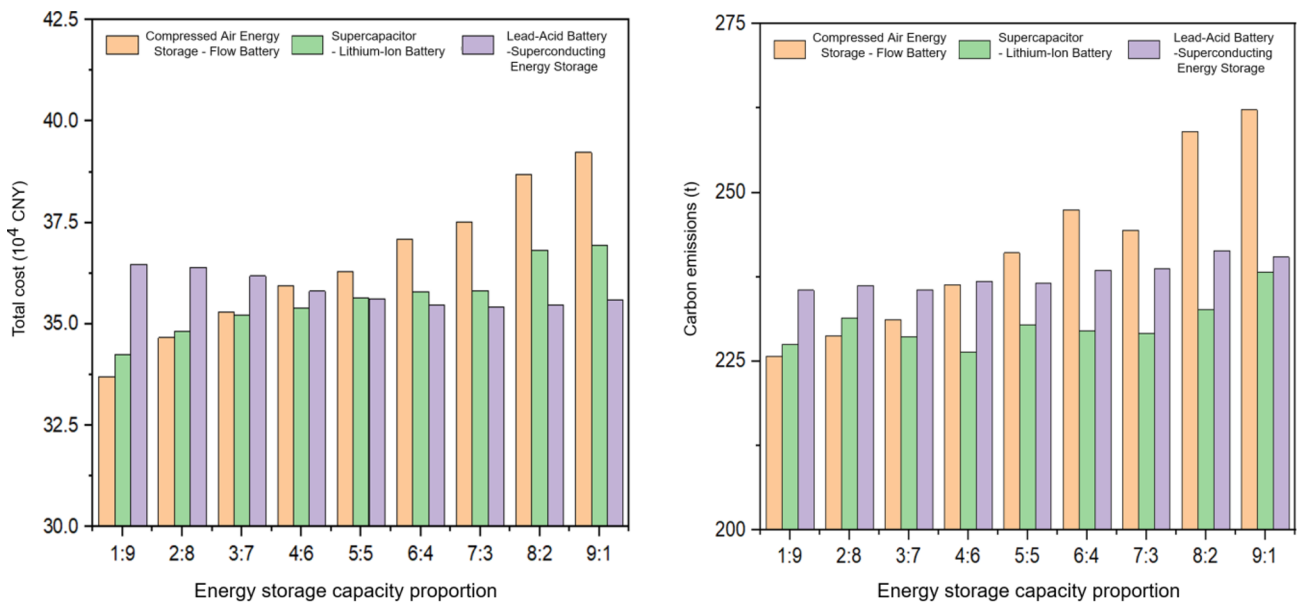


Fig. 8. Relationship between the cost and carbon emissions of the park with different energy storage allocations

power for several hours during the second half of the day, whereas short-term energy storage devices such as superconducting energy storage and supercapacitor energy

supplying energy during periods of high demand in the first half of the day.

Building upon the aforementioned research, the study further explores the impact of changing the energy storage capacity ratio within mixed energy storage on the operating costs and carbon emissions of the three combinations (Fig. 9). The results are as follows:

Among the three different combination types, compressed air energy storage - flow battery (long-term energy storage - long-term energy storage) has the lowest operating costs and energy carbon emissions when the capacity ratio is 1:9. However, as the capacity of compressed air energy storage in the mixed energy storage increases, the costs and carbon emissions of the energy system increase significantly. As the capacity ratio increases to 9:1, the energy system's carbon emissions gradually increase to 262.2 tons, a 16.1% increase compared to 225.8 tons when the ratio is 1:9. Similarly, the operating costs increase from 337,000 yuan to 392,000 yuan, a 16.3% increase. The main reason for the cost and carbon emission increases is that the energy conversion efficiency of current compressed air energy storage technology (45%) is much lower than that of other types of energy storage, resulting in significant energy loss after charging and discharging. Although the cost per kWh of compressed air energy storage is the lowest, its additional costs and carbon emissions are higher due to its low energy efficiency and high self-discharge rate. This combination is suitable for areas with high requirements for energy supply stability, but the current compressed air energy storage technology is still challenging to commercialize.

The combination of supercapacitor batteries - lithium-ion batteries (short-term energy storage - short-term energy storage) shows fluctuations in the overall carbon emissions of the energy

storage can only generate full-load power for a single hour during high-demand periods in the second half of the day. However, due to their high efficiency, they effectively support

system as the proportion of supercapacitors in the mixed energy storage increases. When the capacity ratio changes from 1:9 to 7:3, the overall carbon emissions of the energy system remain within 229.0 tons \pm 2.6 tons. However, as the proportion of supercapacitors in the mixed energy storage continues to increase, the overall carbon emissions will increase sharply. When the proportion of supercapacitors reaches 90%, the carbon emissions of the energy system reach 238.2 tons, a 4% increase compared to 229.1 tons when the proportion is 70%. The main reason for this increase is that although supercapacitors have slightly lower efficiency compared to lithium-ion batteries, the carbon emissions per kWh of lithium-ion batteries are higher than those of supercapacitor energy storage, resulting in initial fluctuations. However, as the proportion of supercapacitors increases, the increase in carbon emissions caused by efficiency becomes dominant, leading to an overall increase in operating carbon emissions. In terms of costs, due to the higher cost per kWh of supercapacitors, the operating costs of the park continue to rise as the proportion of supercapacitors increases, but the increase is relatively small, from 342,000 yuan when the ratio is 1:9 to 369,000 yuan when the ratio is 9:1, an increase of 7.9%.

The combination of lead-acid batteries - superconducting energy storage (long-term energy storage - short-term energy storage) has a minor effect on the carbon emissions of the park when the proportion changes, with only a slight increase from 235.5 tons with lead-acid batteries accounting for 10% to 240.4 tons with lead-acid batteries accounting for 90%, an increase of only 2.1%. This is mainly because lead-acid batteries have a shallow discharge depth, and some energy remains within the energy storage device. Moreover, it has a certain downward trend in terms of costs, decreasing from 365,000 yuan with

lead-acid batteries accounting for 10% to 356,000 yuan with lead-acid batteries accounting for 90%, a decrease of 2.4%. This decrease is mainly due to the increase in short-term energy storage in the mixed energy storage, which helps the energy system obtain energy arbitrage under time-of-use electricity pricing, thereby reducing the operating costs of the energy system. Additionally, the cost reduction is also due to the relatively low cost of lead-acid batteries and their high efficiency, resulting in fewer additional costs. As the proportion of lead-acid batteries increases, the overall costs tend to decrease. This combination balances temporary load peak shaving and load shifting requirements of short-term energy storage types while ensuring the stability of energy supply in the park, enabling the park to have certain capabilities to respond to emergencies

In summary, through comparative studies, the mixed energy storage of lead-acid batteries - superconducting batteries (long-term energy storage - short-term energy storage) exhibits opposite trends in operating costs and carbon emissions under different capacity ratios, requiring a trade-off between costs and carbon emissions for the optimal capacity ratio. Conversely, the combinations of supercapacitors - lithium-ion batteries (short-term energy storage - short-term energy storage) and compressed air energy storage - flow batteries (long-term energy storage - long-term energy storage) should ensure that the most excellent performing energy storage type dominates in the optimal capacity ratio.

6 Conclusions

This study is based on a comprehensive energy system model that encompasses photovoltaic power generation, wind power generation, and CCHP equipment. It investigates the impact of a single energy storage technology on the cost and carbon emissions of this energy system under different scenarios. Building upon this analysis, the study examines the performance, cost, and carbon emission differences of the comprehensive energy system under the mixed application of energy storage, considering the characteristics of different energy storage technologies. The following conclusions are drawn:

1. For this comprehensive system, the appropriate application of energy storage devices can effectively improve the economic feasibility of the energy system. For instance, when using an 8000kWh lithium iron phosphate energy storage battery, the cost per unit of electricity decreases from 0.2747 yuan/kWh (without energy storage) to 0.2729 yuan/kWh.

2. However, this economic improvement is influenced by the instability of wind and solar power generation. According to various capacity configurations designed in this study, the optimal range for short-term energy storage devices such as superconducting energy storage, lithium-ion battery storage, and supercapacitor storage is the maximum value (2000 kWh). Long-term energy storage devices like lead-acid batteries, flow batteries, and compressed air energy storage have an optimal range for different capacity configurations, and this range

varies due to the different characteristics of energy storage and wind/solar characteristics.

3. Further analysis of three different mixed energy storage applications in the comprehensive energy system reveals significant cost differentiation advantages under different energy storage requirements: In the case of compressed air combined with flow battery energy storage, the operating cost is lowest when the proportion of compressed air energy storage is less than 40%. However, as the energy storage capacity increases, the cost of compressed air and flow battery mixed energy storage rises rapidly, surpassing the other two mixed energy storage options. In the 400 kW to 500 kW energy storage demand range, supercapacitor combined with lithium-ion mixed energy storage has the lowest cost advantage. After exceeding 500 kW of energy storage demand, lead-acid combined with superconducting mixed energy storage exhibits the optimal cost advantage. Additionally, different mixed energy storage scenarios have varying impacts on the carbon emissions of the comprehensive energy system. Overall, compressed air combined with flow battery energy storage has the highest carbon emissions impact as its capacity increases, with a 16.1% increase compared to supercapacitor combined with lithium-ion and lead-acid combined with superconducting energy storage, which increased by 4.7% and 2.1%, respectively, as the capacity ratio changed from 1:9 to 9:1.

In conclusion, given the rapid development of energy storage technology and applications, it is necessary to conduct targeted analyses based on the characteristics of different renewable energy generation and energy system load characteristics when selecting energy storage technology and capacity. This approach is crucial for meeting the requirements of the energy system while minimizing the cost and maximizing the utilization of energy storage systems.

7 Funding

We gratefully acknowledge financial support from State Grid Jiangsu Electric Power Design Consulting Co., Ltd Nanjing via JE202106

8 References

1. Shuyin Biao, et al., Study on Low Carbon Energy Transition Path Toward Carbon Peak and Carbon Neutrality. Proceedings of the CSEE, 2023. 43(05): p. 1663-1672.
2. Guo, Y., et al., The Role of Industrial Parks in Mitigating Greenhouse Gas Emissions from China. Environmental Science & Technology, 2018. 52(14): p. 7754-7762.
3. Xu Gang, et al., Strategic Analysis of CO2 Mitigation in Chinese Power Industry. Proceedings of the CSEE, 2011. 31(17): p. 1-8.
4. Ouyang, X. and B. Lin, An analysis of the driving forces of energy-related carbon dioxide emissions in

- China's industrial sector. *Renewable & Sustainable Energy Reviews*, 2015. 45: p. 838-849.
5. National Development and Reform Commission, 《National Carbon Peak Pilot Construction Plan》, p. 14.
 6. Li Jianlin, et al., Summary of Research on Grid-Side Energy Storage Technology. *Electric Power Construction*, 2020. 41(06): p. 77-84.
 7. Zhang Boting, Hydropower and Pumped Storage: Important Guarantees to Achieve Carbon Neutrality. *Hydropower and New Energy*, 2023. 37(04): p. 1-5.
 8. Ma Tingshan, et al., Research Progress on Flexibility Transformation Technology of Coupled Energy Storage for Thermal Power Units Under the "Dual-carbon" Goal. *Proceedings of the CSEE*, 2022. 42(S1): p. 136-148.
 9. Lv Jian, et al., Research on Control Technology of Thermal Power Units Based on Deep Peak Regulation in New Power Systems. *Shanxi Electric Power*, 2023(06): p. 49-53.
 10. Li Xiongwei, et al., A Hierarchical Optimal scheduling Model of Wind-Photovoltaic-Thermal-Energy Storage System Considering Deep Peak Shaving of Thermal Power. *Hydrocarbon and New Energy*, 2023. 35(06): p. 74-81.
 11. Huang Qiuli, Stochastic Economic Dispatch Modeling and Methodology for Coupled Renewable Energy and Thermal Power Systems. 2021.
 12. Zhang Yan, A study of short-term deep peaking of a group of terraced hydropower plants under strong hydraulic linkage.. 2021.
 13. Zhang Juntao, et al., Progress, Challenges and Prospects of Research on Hydropower Supporting the Flexibility of New Power System *Proceedings of the CSEE*: p. 1-22.
 14. Chen Yumeng, Optimal Allocation of Energy Storage Capacity for Wind Energy Storage Systems in Parks, 2023. 13(10): p. 293-295.
 15. Sun Qichao, et al., Optimal Allocation of Energy Storage Capacity for Wind Energy Storage Systems in Parks. *Chemical Industry and Engineering Progress*: p. 1-10.
 16. Wang Liqiang, et al, Research on Participation of Wind-Solar-Storage System in Power Grid Frequency Regulation and Consumption Technology. *Inner Mongolia Electric Power*: p. 1-6.
 17. Xiang Kaiduan, et al., Optimal Capacity Allocation of Wind-solar-storage System with Hybrid Energy Storag. *Science Technology and Engineering*, 2023. 23(31): p. 13415-13422.
 18. Xie Peng, et al., Cooperative Optimization of Energy Storage Capacity for Renewable and Storage Involved Microgrids Considering Multi Time Scale Uncertainty Coupling Influence. *Proceedings of the CSEE*, 2019. 39(24): p. 7126-7136+7486.
 19. Wang, W., et al., Application of energy storage in integrated energy systems - A solution to fluctuation and uncertainty of renewable energy. *Journal of Energy Storage*, 2022. 52.
 20. Le Chengyi, et al, Impact of new energy access on power grid stability and counter measures. *Natural Science Journal of Xiangtan University*, 2022. 44(06): p. 121-126.
 21. Li Bo, et al., A Review of Long-term Planning of New Power Systems With Large Share of Renewable Energy. *Proceedings of the CSEE*, 2023. 43(02): p. 555-581.
 22. Impram, S., S.V. Nese, and B. Oral, Challenges of renewable energy penetration on power system flexibility: A survey. *Energy Strategy Reviews*, 2020. 31.
 23. Gong Yiping, et al., Overview of large-scale energy storage technology and multi-function application. *Distribution and Utilization*, 2023. 40(02): p. 68-77.
 24. Jia Honggang, et al., Study on capacity optimization of hybrid energy storage system based on particle swarm algorithm. *Automation & Instrumentation*, 2023(10): p. 282-287.
 25. Yang Guohua, et al., Capacity optimization of hybrid energy storage based on improved PSO algorithm. *Electrical Measurement & Instrumentation*, 2015. 52(23): p. 1-5+10.
 26. Li Lianbing, et al., Capacity Optimization of Hybrid Energy Storage Based on Improved Immune Particle Swarm Optimization Algorithm. *Journal of Power Supply*: p. 1-14.
 27. He, Y., et al., Multi-objective planning-operation co-optimization of renewable energy system with hybrid energy storages. *Renewable Energy*, 2022. 184: p. 776-790.
 28. Akram, U., M. Khalid, and S. Shafiq, Optimal sizing of a wind/solar/battery hybrid grid-connected microgrid system. *Iet Renewable Power Generation*, 2018. 12(1): p. 72-80.
 29. Jiang Haiyang, et al., Review and Prospect of Seasonal Energy Storage for Power System with High Proportion of Renewable Energy. *Automation of Electric Systems*, 2020. 44(19): p. 194-207.
 30. Wu zhen, et al., Seasonal Energy Storage Capacity Planning for Provincial Region Considering Unbalanced Seasonal RenewableEnergy Generation. *Electric Power*, 2023. 56(08): p. 40-47.
 31. Converse, A.O., Seasonal Energy Storage in a Renewable Energy System. *Proceedings of the Ieee*, 2012. 100(2): p. 401-409.
 32. Yuan Guili, et al., Measures for Large-Scale New Energy Generation Consumption. *Advances in New and Renewable Energy*, 2017. 5(04): p. 305-314.
 33. Zhang Ziyang, et al, International competition of key energy storage technologies based on high-quality patents. *Energy Storage Science and Technology*, 2022. 11(01): p. 321-334.

34. Gong Daoren, et al, Mathematics calculation model and application of CO2 emission. *Renewable Energy Resources*, 2013. 31(09): p. 1-4+9.
35. Zhang Kaizhen, et al., Research Progress on Characteristics Analysis and Optimization Control of Cogeneration System. *Advances in New and Renewable Energy*, 2019. 7(02): p. 168-175.
36. Yin Yongjie, et al, Benefit Evaluation and Operation Strategy of CCHP. *Electric Engineering*, 2019(19): p. 11-14+18.
37. Li YongGuang, et al., Optimal Operation of Integrated Electricity-heat Energy System Considering Wind Power Consumption. *Power Capacitor & Reactive Power Compensation*, 2021. 42(05): p. 228-235.
38. Ou Yangbin, et al., Storage Multi-Energy Complementarity Research on Optimal Operation of Cold-Thermal-Electric Integrated Energy System Considering Source-Load. *Power Generation Technology*, 2020. 41(01): p. 19-29.
39. Ni Long, et al., Carbon reduction benefits of heat pump in medium-low temperature heat production, *Heating Ventilating & Air Conditioning*, 2022. 52(11): p. 23-34.